Analysis and Design of a 20 MHz Bandwidth, 50.5 dBm OOB-IIP3, 5.4mW TIA for SAW-Less Receivers

Giacomo Pini, *Student Member, IEEE*, Danilo Manstretta, *Member, IEEE*, and Rinaldo Castello, *Fellow, IEEE*

***Abstract*—A power-efficient trans-impedance amplifier (TIA) with wide channel bandwidth is proposed to meet the stringent linearity requirements of SAW-less frequency-division duplexing (FDD) receivers. A unity-gain loop bandwidth of 1.6 GHz is achieved with low power dissipation. This was done without using any internal compensation but relying on zeros, both within the operational transconductance amplifier and in the feedback network, to ensure stability across all parameter variations. A simple nonlinear analysis methodology is presented that provides important insights, useful for the design optimization. The prototype, implemented in 28nm CMOS technology, has 14dB of gain with 20MHz bandwidth and achieves 21.1μV in-band noise together with 33 dBm and 50.5 dBm IIP3 at 6 MHz and 100 MHz offset respectively, while requiring only 5.4mW. The corresponding filter figure of merit of 183.2 dBJ^{-1} at 100 MHz offset exceeds that of all previous designs. Simulation shows that an even better FOM could be achieved using a larger width (more linear) feedback resistor. Finally, the differential input impedance is less than 33 Ohm at all frequencies.**

***Index Terms*—Baseband, Frequency-Division Duplexing, high linearity, low-power, mobile receivers, SAW-less, TIA.**

I. Introduction

NEWER communication standards for both cellular and Wi-Fi applications use wider channel bandwidths. At the same time, the attempt to reduce cost by removing some off-chip filters and the need to co-exist with other transceivers on the same board, increases the required linearity of the receiver. In either Frequency-Division Duplexing (FDD) or Full-Duplex (FD) systems, the use of Self-Interference Cancellation Techniques can significantly reduce the required linearity [1]-[4]. Nonetheless, residual interference is still larger than when using highly selective off-chip filters. Whereas both the IIP3 and compression of the receiver front-end has been extensively studied [5], less attention was given to the base-band (BB) portion. For the universally used current-mode receiver architecture [6], the first block after the passive mixer is either a filtering trans-impedance amplifier (TIA) or a higher order filter [6]-[11]. In both cases, very stringent requirements are placed on this circuit. For FDD, it needs to have high out-of-band (OOB) linearity and low input impedance up to very large offset frequencies, while for FD, high in-band (IB) linearity and wide bandwidth are needed. In both cases, low integrated IB noise and small area with the smallest possible power consumption are desired. Placing a very large capacitor (hundreds of pF) on the virtual ground node helps with some of these issues but it increases area and integrated noise. In literature many continuous time filters with bandwidth of up to tens of MHz are presented [12]-[19]. Although some have good Dynamic Range (DR)[15], they do not always address all the specs of a BB channel filter, e.g. low input impedance. In [20][21] a receiver BB TIA is enhanced by placing a negative resistance in parallel with its input nodes. In [21] this is exploited to significantly improve the IB IIP3, but with small benefits on the OOB IIP3 and at the cost of extra noise and power consumption. Lower noise is achieved in a TIA [13] that uses a smaller input capacitance by boosting its value for OOB signals. Furthermore, a second order filtering is implemented which is beneficial for the following stages. However, its relatively high input impedance may degrade the mixer linearity. These limitations could be overcome if the TIA/filter were able to achieve high IB IIP3 and to maintain both low input impedance and high IIP3 up to high frequencies. Many active-RC filters for channel-selection use a simple Two-Stage operational trans-conductance amplifier (OTA) with Miller compensation [11][12][16][22], which suffers from a low gain-bandwidth product when loaded with a large capacitor. In [23] a filtering TIA based on a Three-Stage OTA showing high gain over a large bandwidth and enabling good virtual ground and high linearity was presented. This was achieved using a non-classical approach to compensation. No Miller capacitors were used but stability was ensured thanks to some additional zero's introduced within both the forward and feedback portion of the loop. In this work, an OTA non-linearity modeling is proposed, that is then applied to the analysis of the TIA. An extended design section is presented, including a detailed stability analysis. The paper is organized as follows. After this introduction, the key target specifications of the TIA are

This paragraph of the first footnote will contain the date on which you submitted your paper for review. It will also contain support information, including sponsor and financial support acknowledgment. For example, "This work was supported in part by the U.S. Department of Commerce under Grant BS123456."

G. Pini, D. Manstretta and R. Castello are with the Department of Electrical, Computer and Biomedical Engineering, University of Pavia, Pavia, Italy (e-mail: giacomo.pini01@universitadipavia.it; danilo.manstretta@unipv.it; rinaldo.castello@unipv.it).

derived in Section II. Section III describes the design of the uncompensated three-stage OTA. The model used to analyze the non-linearities of the TIA is introduced in Section IV. The design of the uncompensated three-stage OTA is given in Section IV and experimental results on the TIA prototype in Section V, with also some insights on a Self-Interference Cancellation Receiver the TIA was included in. Some conclusions are drawn in Section VI.

II. TIA Target Specifications

When a TIA is driven by a passive current-switching mixer, a big capacitor C_{in} is always placed at its input nodes [8][10][11] (Fig. 1). This serves several purposes. 1) It shunts the signal at the clock harmonics. 2) It maintains low input impedance across frequency to preserve both mixer IIP2 and IIP3 with strong OOB interferers [24]. 3) It filters the higher frequency down converted interferers, improving TIA OOB IIP3. To fulfill all these requirements, increasing the value of C_{in} is beneficial and typically C_{in} is of the order of 200 pF [8][10]. A large C_{in} has, however, the drawback of increasing both area and noise. In fact, the noise transfer function (NTF) of the OTA input-referred noise voltage is proportional to $|1+Z_F/Z_{in}|^2$, where Z_F is the feedback impedance and Z_{in} is the virtual ground impedance, i.e. the parallel of C_{in} and the driving impedance R_d. Hence, C_{in} creates a zero in the OTA NTF at $1/(R_dC_{in})$ and, if this falls within the signal bandwidth, the integrated noise degrades. For example, assuming R_d=500 Ω [25][26] and that the filter bandwidth ω_0 is 15 MHz, a 20 pF C_{in} produces a NTF zero at ω_0 and 1.2 dB increase in the integrated OTA noise. Beyond this value, however, the integrated noise increases with the square of C_{in}, quickly becoming unacceptable. We, therefore, need to find an optimum value for C_{in}. With respect to point 1 above, we see that the impedance of a 20 pF C_{in} is significantly smaller than the switches on-resistance R_{ON} (typically about 20Ω) even at the lowest possible harmonic of the LO. Therefore, from this point of view, we have no reason to increase C_{in} beyond 20 pF. With respect to point 2 above, we need to ensure that the TIA input impedance Z_{in} remains below R_{ON} up to the highest blocker frequency (e.g. 400 MHz for LTE in FDD). Z_{in} is the parallel of C_{in} and the TIA impedance at its virtual ground Z_{VG}. Since 20pF correspond to 20Ω at 400MHz, a much higher C_{in} or a very broadband OTA are required to satisfy the above requirement at all frequencies. In this paper we target a sufficiently wideband OTA to achieve low Z_{in} at all frequencies with a C_{in} of 20pF, to avoid noise penalties. With respect to point 3 above, if the impedance of C_{in} is lower than Z_{VG} at the blocker frequency, only a fraction of the blocker current is absorbed by the OTA. On the other hand, with a C_{in} of 20pF, all the blockers are absorbed by the OTA, making OTA IIP3 much more critical. To design an highly linear OTA we need a model of the distortion associated with its different stages.

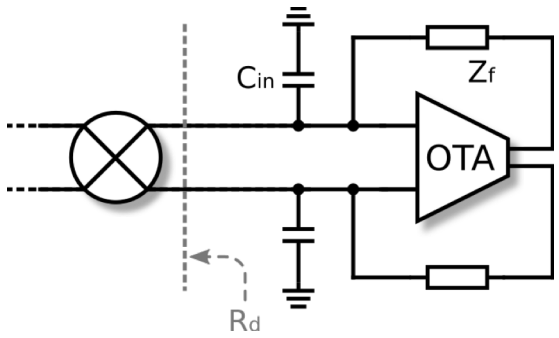

Fig. 1. Typical TIA with big input capacitance

III. OTA Design

In order to extend OTA bandwidth and achieve low TIA input impedance over a broad bandwidth with 20 pF C_{in}, an unconventional approach was adopted to ensure loop stability. In traditional general-purpose OTA design, where purely capacitive load is assumed, Miller compensation schemes are often used. Miller capacitors create one dominant pole in the OTA transfer function and push non-dominant poles above the unity gain bandwidth (GBW), increasing phase margin and guaranteeing OTA stability. In the design of BB TIAs such approach has the main drawback of producing a low frequency pole, limiting OTA bandwidth and making TIA input impedance increase. In fact, the GBW is limited to about one half of the non-dominant pole, which is given by the ratio between the last stage transconductance and the effective load capacitance C_{in}. To gain a quantitative insight, targeting a GBW of 1.6 GHz with a 20 pF load capacitance, would require an unpractically high transconductance of 400 mS. In our solution no Miller capacitors are used. Stability is instead achieved by placing some additional zeros in the TIA loop gain, both in OTA and feedback network transfer functions, close to GBW to improve phase margin. This approach allows achieving much wider OTA bandwidth than a Miller compensation. In the following a detailed OTA description is provided. The OTA architecture is given in Fig. 2 and design parameters in Table I. The First Stage consists of a PMOS Telescopic-Cascode, with

TABLE I
OTA Design Parameters

Parameter	Value
M1,M2	140/0,08
Mc1, Mc2	20/0,04
Mc3, Mc4	8/0,04
M3, M4	20/0,2
M5,M6	20/0,06
M7,M8, M9, M10	2/0,08
M11, M12	6/0,08
MPo+, MPo-	36/0,08
MNo+, MNo-	16/0,08
M13, M14	12/0,08
C_c	300 fF
R_c	500 Ω
R_{deg}	250 Ω
R_z	1 kΩ
C_z	100 fF

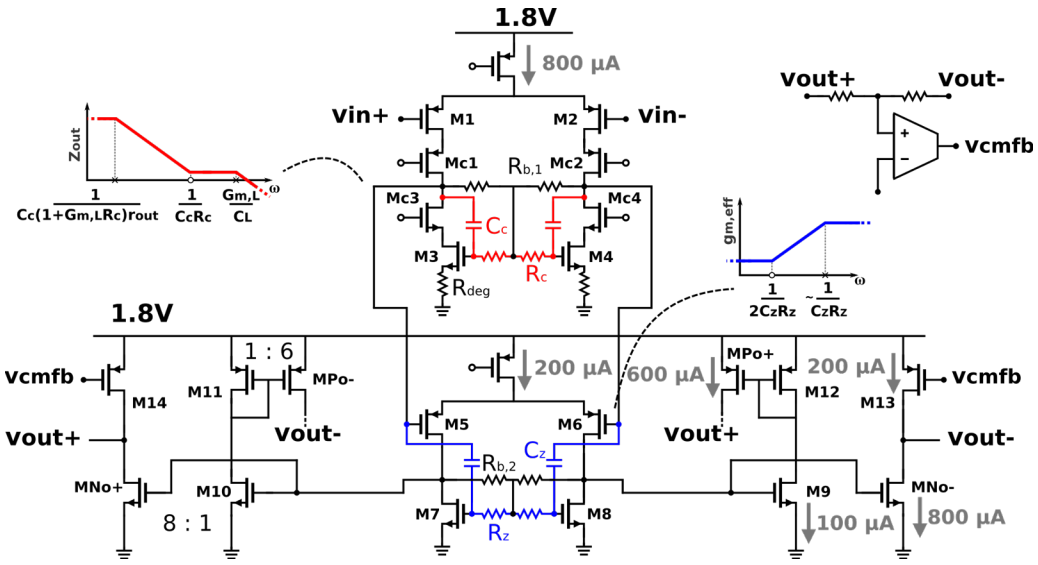

Fig. 2. Schematic of the proposed OTA

R_c and C_c providing an output impedance $Z_{O,1} = r_{out,1} // \frac{1}{sC_{L,1}} // \frac{1+j\omega R_c C_c}{j\omega C_c(1+G_{m,L}R_c)}$, where $r_{out,1}$ is the output resistance at low frequency, $C_{L,1}$ is the output capacitance and $G_{m,L}$ is the equivalent trans-conductance of the load transistors M3/4 degenerated by R_{deg}. The third term is associated with R_c and C_c and corresponds to the series combination of capacitance $C_c(1+G_{m,L}R_c)$ and resistance $R_c/(1+G_{m,L}R_c)$. $Z_{o,1}(\omega)$ has a low-frequency pole $\omega_{p,OTA,1} = 1/C_c(1+G_{m,L}R_c)\cdot r_{out,1}$ and a high-frequency zero $\omega_{z,OTA,1} = 1/(R_cC_c)$ that is placed before the TIA GBW to improve phase margin. At very high frequency $C_{L,1}$ produces a second pole $\omega_{p,OTA,2} \approx G_{m,L}/C_{L,1}$. The common-mode (CM) output voltage is set by the local feedback made, at low frequency, by $R_{b,1}$ and, at high frequency, by C_c. The second stage is a PMOS differential pair, with the boosting network R_z, C_z which produces a zero-pole doublet $\omega_{z,OTA,2} = 1/(R_zC_z(1+g_{m,7/8}/g_{m,5/6}))$ and $\omega_{p,OTA,3} = 1/(R_zC_z)$. This is because above $\omega_{p,OTA,3}$, capacitance C_z shorts the gate of $M_{5/6}$ and $M_{7/8}$ approximately doubling the stage g_m. In addition there is a pole $\omega_{p,OTA,4} = 1/r_{o,2}C_{L,2}$, where $r_{o,2}$ and $C_{L,2}$ are the resistance and capacitance at the output which is, however, cancelled placing $\omega_{z,OTA,2}$ on top of it. In this way the stage shows a single pole at $\omega_{p,OTA,3}$. The CM voltage of the second stage and the DC current in the output stage is set through $R_{b,2}$. The output stage is based on a crossed current mirror where the NMOS transistors ($M_{O,N+/-}$) are driven directly while the PMOS ($M_{O,P+/-}$) are driven through the mirror made of M9/10 and M11/M12. In this design, the output stage was enlarged compared with what would be required in normal operation, to directly drive the big off-chip capacitance (C_L), without using a buffer. The output CM is set to 900 mV with a CM Feedback (CMFB) loop that controls the P-side current in the output branches (transistors M13/14) via a resistor divider and a simple OTA.

A. TIA Stability

The complete TIA is reported in Fig. 3.a. Even if it was implemented in differential form, single-ended representation of the TIA is used here for simplicity. C_L represents the testing probe input capacitance, which is about 2 pF (differential) and is represented here as a single-ended 4 pF-capacitance. In a real receiver the actual load seen by the TIA would be drastically smaller, i.e. below 100 fF. A smaller load results in a better linearity for the same OTA since the output stage needs to deliver less current. This means that the measured IIP3 is smaller than the one achievable in the real receiver. Through simulation 6 dB improvement in OOB IIP3 was demonstrated with 100 fF load capacitance. R_{in} in series with C_{in} and R_L in series with C_L are added to improve stability, as discussed below. However, to filter out clock harmonics, the input signal is injected below R_{in}. The loop gain is computed breaking the loop at the input of the OTA, injecting a test signal v_t and observing the return signal v_r, as shown in Fig. 3.b. The singularities of the OTA first and second stage were derived previously and the simulated transfer functions of these stages are reported in Fig. 4.a, where poles and zeros were highlighted for clarity. The high-frequency zero of the first stage $\omega_{z,OTA,1}$ is placed before the second stage pole $\omega_{p,OTA,3}$ to improve phase margin. Poles and zeros introduced by third stage and feedback network are listed below assuming R_L and R_{in} are much smaller than all other resistances and $C_{in} >> C_F$, C_L. In Fig. 4.b the simulated transfer function of the output stage and passive feedback network, i.e. $v_r/v_{o,2}$ in Fig. 3.b, is reported. A low-frequency pole is produced by C_{in} at frequency $\omega_{p,4} = 1/(R_d//(R_F+r_o)C_{in})$, R_{in} gives a high frequency zero at $\omega_{z,4} = 1/R_{in}C_{in}$, which is placed before the GBW. This is key to ensure stability given the two low-frequency poles ($\omega_{p,OTA,1}$,$\omega_{p,4}$). Feedback components create a zero at $\omega_{z,3} = 1/R_FC_F$ and a pole at $\omega_{p,5} = 1/(R_f//r_o)(C_F+C_L)$, near the cut-off frequency. The large external load capacitance C_L significantly reduces $\omega_{p,5}$. Increased OTA bandwidth could be achieved using an on-chip buffer or additional filtering stage as load. R_L creates a high-frequency zero-pole doublet at $\omega_{z,5} = 1/(R_LC_L)$ and $\omega_{p,6} =$

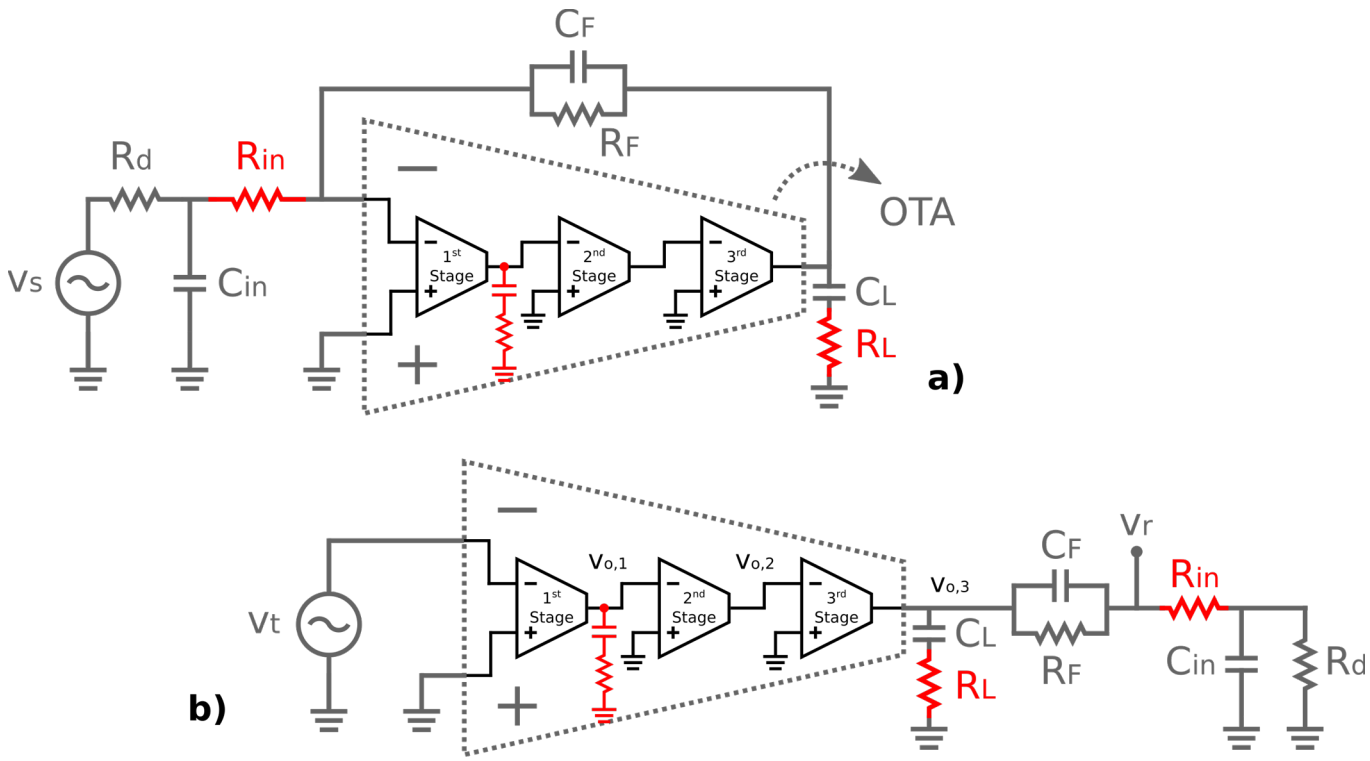

Fig. 3. a) Simplified single-ended representation of the proposed TIA Architecture. b) Open-Loop circuit used to compute the loop gain.

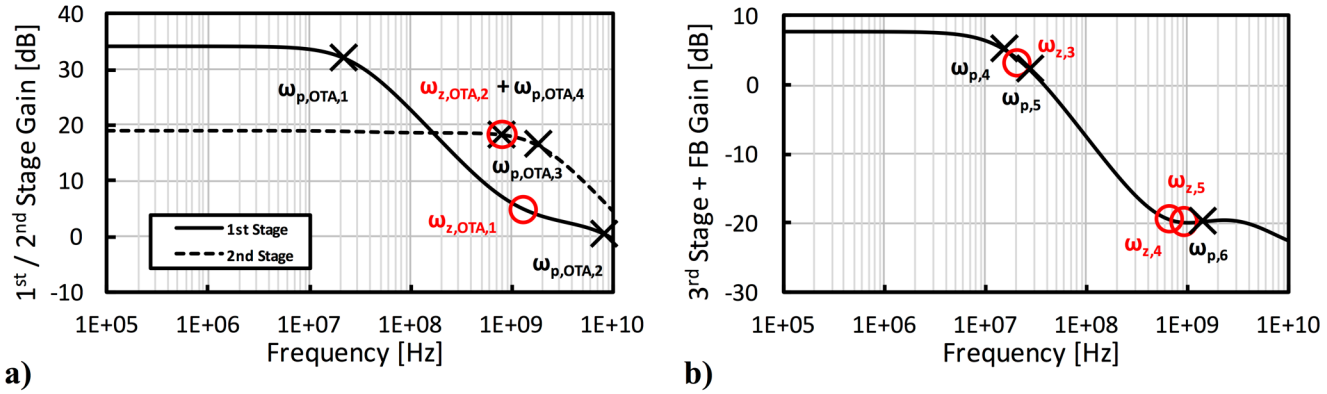

Fig. 4. a) Gain of 1st (solid line) and 2nd (dashed line) Stage. b) Gain of 3rd Stage and passive feedback network.

$(C_F+C_L)/(C_FC_L(R_{in}+R_L))$. For the components given in Table II the post-layout simulated magnitude and phase of the loop transfer function is shown in Fig. 5 (black curve). The loop has a gain of nearly 60 dB at DC which remains flat up to the feedback pole $\omega_{p,4}$, located around 18 MHz. Next we find the first stage pole $\omega_{p,OTA,1}$, at 20 MHz, followed by the zero-pole pair $\omega_{z,3}$-$\omega_{p,5}$, near 20 MHz and 32 MHz respectively. Beyond 32 MHz the curve starts decreasing with a slope of 40 dB/decade. Above $\omega_{z,4}$, located at 670 MHz, 20 dB/decade slope is resumed. Since $\omega_{z,OTA,1}$ (at about 1.1 GHz) is very close to $\omega_{p,OTA,3}$ the plot crosses the 0-dB axis with slightly less than 20 dB/dec slope at 1.5 GHz GBW, in the vicinity of the zero-pole doublet given by R_L and C_L ($\omega_{z,5}$ and $\omega_{p,6}$). At GBW the phase is close to its maximum, giving 57° of phase margin. TIA stability was simulated over all process corners and for different operating temperatures, including passive components variations. Singularity position is affected by the MOM capacitors and Poly-silicon resistors used in the feedback network and within the OTA. Having such passives low temperature coefficients (few hundreds ppm/°C), PM and GBW are stable across temperature as shown in Table III, reporting simulated PM and GBW over all process corners and for different temperatures. Fig. 5 shows the phase and magnitude response of the loop for extreme values of temperature and

process demonstrating stability robustness. The most critical corner is Slow-Slow (SS) where salicided poly-silicon resistor R_{in} strong variations lower $\omega_{z,4}$, increasing GBW to give 42° of PM. Montecarlo simulation over 500 samples defines the effect of the mismatch. A standard deviation of 176 MHz in GBW and of 2.5° PM is obtained. From the point of view of the mixer load, we see that the virtual ground impedance stays below the switches Ron up to 400 MHz as required since the OTA gain is higher than 30 dB up to such a frequency. The only open point is the linearity of the TIA itself in the band of interest (i.e. up to 400 MHz) when 20 pF are used at its input.

TABLE II
TIA DESIGN PARAMETERS

Parameter	Value
R_d	500 Ω
C_{in}	20 pF
R_{in}	13 Ω
C_F	3 pF
R_F	2.5 kΩ
C_L	4 pF
R_L	50 Ω

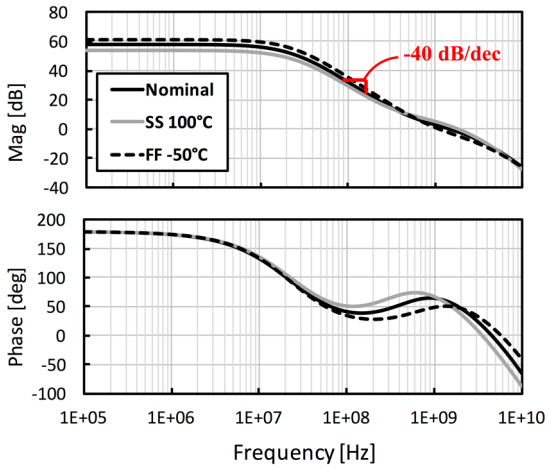

Fig. 5. Loop Gain Magnitude and Phase on Nominal corner (black line), Slow-Slow corner at 100°C (gray Line) and Fast-Fast corner at -50°C (dashed Line)

IV. NON LINEARITY ANALYSIS

This section presents the nonlinearity analysis of the proposed TIA. We introduce a relatively simple model of the closed-loop OTA 3rd order intermodulation (IM3), which is the critical spec in a receiver. 2nd order intermodulation is neglected, assuming a differential structure for the OTA. The model provides three key pieces of information versus tone frequencies and IM3 frequency (f_{IM3}): 1) the total closed loop intermodulation; 2) the stages that dominate distortion in a frequency range; 3) the mechanism that dominates distortion within a stage. Two key concepts are identified: distortion injection and distortion compression. The former represents the distortion a stage injects in the circuit, which depends on the *voltage swing at the intermediate nodes at the frequency of the input tones*. The latter, quantifies by how much the distortion is reduced by the loop, which depends on the *loop gain at the IM3 frequency*. The approach is based on the one proposed in [27]-[30], where the linearized circuit response is used to extract the non-linear terms injected at the various nodes, which are then referred to the output. A single-ended representation of the loop for a Three-Stage-OTA with no internal feedbacks[1] is given in Fig. 6. Each OTA stage is modeled as a trans-conductor ($g_{m,i}$), loaded by $Z_{o,i}$, which includes both output resistance and capacitance. To simplify the analysis, the nonlinearity is modelled at the OTA stage level, as opposed to the transistor level as in [27-29]. Furthermore, only two distortion terms are considered, the first due to the trans-conductance $g_{m,3}$ and the second to the output conductance $g_{ds,3}$. The procedure to get the output intermodulation is represented by the flowchart of Fig. 7 and will be applied to the OTA in Fig. 2. Some parameters must be first computed for each stage by either simulation or computation. In Step 1.a, the non-linear coefficients $g_{m,3,i}$ and $g_{ds,3,i}$ are found simulating each stage separately, as described in Appendix A, giving the results reported in Table IV[2]. In Step 1.b the closed-loop swing versus frequency at the input and output of each stage is obtained. Finally, the closed-loop output impedance $Z_{o,CL,i}$, at the IM3 frequency (f_{IM3}) is computed by dividing the open loop output impedance $Z_{o,OL,i}$ by the loop gain.[3] The output intermodulation contributed by each stage is computed in Steps 2 to 5. In Step 2 the intermodulation injection is found. Applying two sinusoids of amplitude $A_{1,i}$ and $A_{2,i}$ and

TABLE III
TIA CORNER STABILITY

Corner	TT			FF			SS			FS			SF		
Temperature [°C]	-50	25	100	-50	25	100	-50	25	100	-50	25	100	-50	25	100
GBW [GHz]	1.55	1.53	1.5	1.17	1.09	1.03	2.01	1.98	1.9	1.31	1.28	1.27	1.94	1.85	1.76
PM [deg]	58.1	57.6	57.6	50	52	54.5	45.3	42.5	41.3	59.3	60.5	61.6	51.5	51	51.5

[1] The same methodology can be easily applied to other common OTA topologies.

[2] In multi-stage and feedback amplifiers, 2nd order non-linearities coming from two stages may interact, resulting into 3rd order non-linearity. In this design, however, since the first two stages are fully-differential, at least up to very high frequencies, this effect is negligible.

[3] Notice that $Z_{o,OL,3}$ also includes the loading of the feedback network.

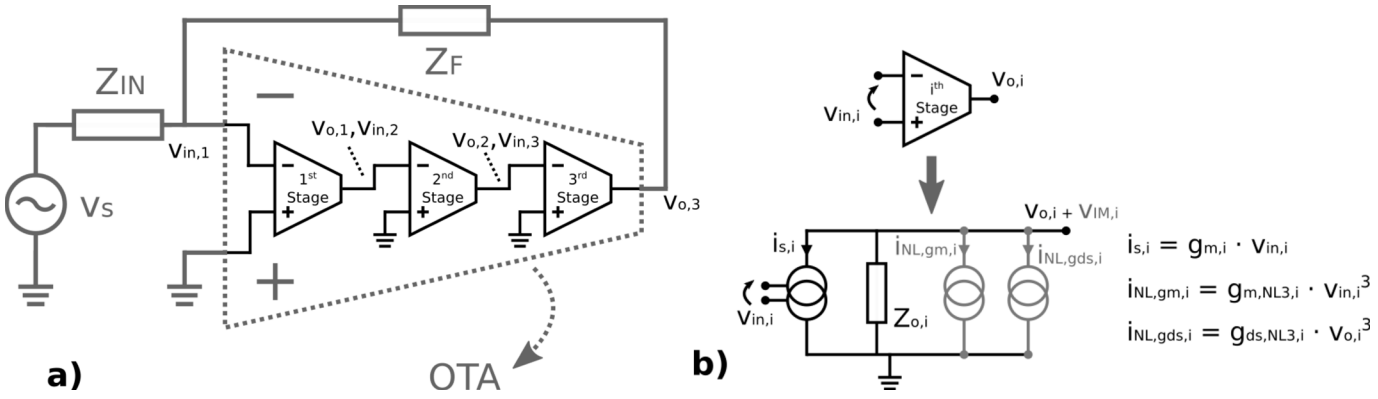

Fig. 6. Simplified Single-ended representation of the proposed model: a) Overall loop; b) Single OTA Stage;

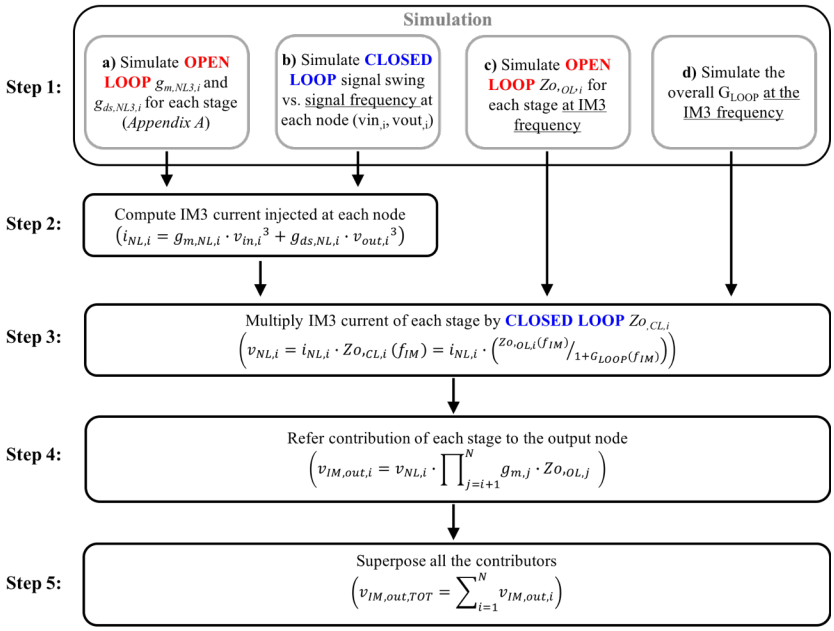

Fig. 7. Schematic representation of the adopted procedure for computation of output intermodulation of an OTA closed in feedback loop

TABLE IV
MODEL COEFFICIENTS FOR THE PROPOSED OTA

Stage	Coefficient	Value
1st	$(3/4) \cdot g_{m,NL,1}$	$3{,}22 \cdot 10^{-2}$ A/V^3
	$(3/4) \cdot g_{ds,NL,1}$	$3{,}58 \cdot 10^{-6}$ A/V^3
	$Z_{o,OL,1}$(1 MHz)	16,4 kΩ
	$TF_{1\to OUT}$(1 MHz)	41,1 dB
2nd	$(3/4) \cdot g_{m,NL,2}$	$9{,}32 \cdot 10^{-3}$ A/V^3
	$(3/4) \cdot g_{ds,NL,2}$	$-7{,}11 \cdot 10^{-6}$ A/V^3
	$Z_{o,OL,2}$(1 MHz)	10,4 kΩ
	$TF_{2\to OUT}$(1 MHz)	22 dB
3rd	$(3/4) \cdot g_{m,NL,3}$	$1{,}19 \cdot 10^{-3}$ A/V^3
	$(3/4) \cdot g_{ds,NL,3}$	$2{,}32 \cdot 10^{-5}$ A/V^3
	$Z_{o,OL,3}$(1 MHz)	2,1 kΩ
	$TF_{3\to OUT}$(1 MHz)	0 dB
	G_{LOOP}(1 MHz)	61,4 dB

frequency ω_1 and ω_2, the two IM3 components in the ith stage output current are located at $2\omega_1 - \omega_2$ and have strengths that depend on the signal amplitude at the input and output of the ith stage as given in (1) and (2).

$$i_{gm,i}^{NL} = \frac{3}{4} g_{m3,i} {A_{1,i}}^2 A_{2,i} \sin\left((2\omega_1 - \omega_2)t\right) \quad (1)$$

$$i_{gds,i}^{NL} = \frac{3}{4} g_{ds3,i} \left(A_{1,i} \cdot |G_i(\omega_1)|\right)^2 \cdot \left(A_{2,i} \cdot |G_i(\omega_2)|\right) \sin\left((2\omega_1 - \omega_2)t + 2\angle G_i(\omega_1) - \angle G_i(\omega_2)\right) \quad (2)$$

where $G_i(\omega_k)$ is the gain of the stage at frequency ω_k and $g_{m3,i}$ and $g_{ds3,i}$ are the third order non-linear coefficients associated with g_m and g_{ds}. In Step 3, the IM3 voltage ($v_{IM,i}$) at the output of each stage, is found by multiplying the total injected current $i_{,NL,gm,i} + i_{,NL,gds,i}$ by the closed loop output impedance $Z_{o,CL,i}$ at f_{IM3} as given in (3). In (3) we add the two non-linear terms, without considering their relative phase, assuming that one term

dominates in each frequency interval. In Step 4, all $v_{IM,i}$ are referred to the output by multiplying them by $TF_{i\text{-}out,}$ i.e. the open loop transfer function from the i[th] stage output to the OTA output. $TF_{i\text{-}out}$ is equal to the product of $g_{m,j} \cdot Z_{o,OL,j}$ at the IM3 frequency for all stages following i[th] stage, as given in (4). In Step 5 all output-referred terms are summed as in (5).

$$v_{IM,i} \cong \left(\frac{3}{4} g_{m,NL3,i} {A_{1,i}}^2 A_{2,i} + \frac{3}{4} g_{ds,NL3,i} \left(A_{1,i} \cdot |G_i(\omega_1)|\right)^2 \cdot \left(A_{2,i} \cdot |G_i(\omega_2)|\right)\right) \cdot \frac{|Z_{o,OL,i}(2\omega_1-\omega_2)|}{|1+G_{LOOP}(2\omega_1-\omega_2)|} \cdot \sin\left((2\omega_1-\omega_2)t\right) \quad (3)$$

$$v_{IM,out,i} = v_{IM,i} \cdot TF_{i\to OUT} = v_{IM,i} \cdot \prod_{j=i+1}^{N} g_{m,j} \cdot Z_{o,OL,j} \quad (4)$$

$$v_{IM,out,TOT} = \sum_{i=1}^{N} v_{IM,out,i} \quad (5)$$

Fig. 8 plots IM3 vs. the first tone frequency for two -20 dBm input signals when the IM3 falls at 1 MHz. The difference between calculations and simulations is typically around 1 dB and always below 4 dB. Fig. 8 shows also the calculated IM3 of each stage. We see that: 1) the last stage dominates distortion up to 400 MHz; 2) beyond this the first stage dominates; 3) when the first stage starts to dominate, the overall IM3 starts to decrease with frequency; 4) the second stage never dominates distortion. This behavior can be intuitively understood as follows. For the last stage, whose $v_{IM,out,3}$ is given in (6), the injected distortion depends only on the output stage itself and not on any other OTA characteristic. This is because both the swing and the current at the output node are set only by the feedback network and the load impedance. The output distortion $v_{IM,out,3}$ is obtained by multiplying the injected distortion by the closed loop output impedance at f_{IM3}.

$$v_{IM,out,3} = \left(i_{gm,3}^{NL} + i_{gds,3}^{NL}\right) \cdot \frac{Z_{o,OL,3}(f_{IM})}{1+G_{LOOP}(f_{IM})} \cong \left(i_{gm,3}^{NL} + i_{gds,3}^{NL}\right) \cdot \frac{1+Z_F/Z_{in}}{g_{m,3} \cdot g_{m,1} Z_{o,OL,1}(f_{IM}) \cdot g_{m,2} Z_{o,OL,2}(f_{IM})} \quad (6)$$

We conclude that, to improve the closed-loop intermodulation distortion of the output stage, it is key to enhance the gain of the OTA *at the IM3 frequency* i.e. up to TIA cut-off frequency ω_0 since intermodulation is increasing the noise floor when it falls within the signal bandwidth. Since the second stage has a broad-band gain of about 20 dB, the swing at its input stays low and constant with frequency, making its distortion always negligible compared to that of the last stage[4]. The first stage distortion is given by:

$$v_{IM,out,1} = \left(i_{gm,1}^{NL} + i_{gds,1}^{NL}\right) \cdot \frac{Z_{o,OL,1}(f_{IM}) \cdot g_{m,2} Z_{o,OL,2}(f_{IM}) \cdot g_{m,3} Z_{o,OL,3}(f_{IM})}{1+G_{LOOP}(f_{IM})} \cong \left(i_{gm,1}^{NL} + i_{gds,1}^{NL}\right) \cdot \frac{1}{g_{m,1}} \cdot \left(1 + \frac{Z_F}{Z_{IN}}\right) \quad (7)$$

The first stage distortion starts from a very small value and rises beyond the first OTA pole at 20 MHz with a 60dB/decade slope since, as the gain $A(\omega_{1,2})$ drops, the virtual ground signal

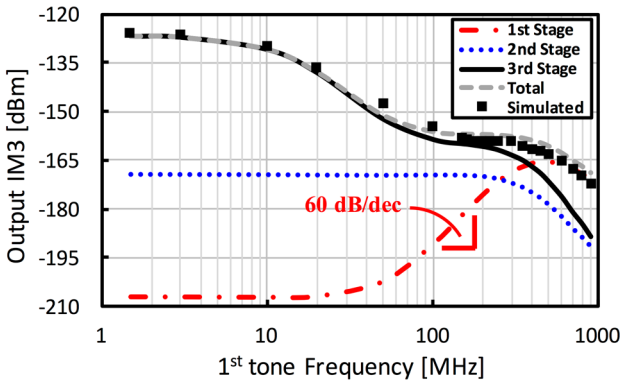

Fig. 8. Simulated and computed IM3 at the TIA output as a function of the input tones frequency, with the proposed OTA and contribution of single OTA stages.

increases as $1/A(\omega_{1,2})$ and the distortion increases as $1/(A^2(\omega_1)A(\omega_2))$. Since OTA gain at 400 MHz is still 30 dB, OTA input swing stays small enough to prevent excessive distortion injection in this range. The situation is the dual of the output stage. For a given input stage, distortion compression by the loop is independent from any characteristic of the OTA. On the contrary, *distortion injection decreases increasing the OTA gain at the tone frequency*. We conclude that, to improve the closed-loop intermodulation distortion of the input stage, it is key to enhance the gain of the OTA *at the frequency of the OOB tones* i.e. up to maximum frequency distance between TX and RX band. Alternatively, C_{in} can achieve the same goal thanks to its low pass filtering effect at the OTA input. Notice, however, that C_{in} cannot be increased arbitrarily since this may not only degrade noise but can also have an adverse effect on output stage linearity. In fact, when C_{in} is large enough to lower Z_{in} before the TIA cut-off frequency ω_0, the loop gain starts to decrease in band due to a reduction of the feedback factor and the IM3 of the output stage increases as its frequency nears ω_0. In this design C_{in} starts diverting the current from the OTA around 400 MHz, making overall IM3 to decrease with frequency.

Our method allows also to find which distortion mechanism dominates within a stage. This information is difficult to obtain even using sophisticated distortion simulations [31]. Focusing on the output stage, we see from Fig. 9 that, at low frequency, the large output swing makes g_{ds} non-linearity dominant. As a result, the output IM3 follows the frequency response of the TIA i.e. beyond ω_0 it decreases with a slope of 60dB/decade, leading to a sharp rise in the IIP3. Around 60 MHz the g_m non-linearity takes over and IM3 flattens out, leading to a plateau in the IIP3. This is because up to 400 MHz the input current is completely absorbed by the OTA, hence both the swing at the input of the last stage and the g_m nonlinearity are frequency independent. On the other hand, at higher frequency C_{in} absorbs part of the input current, lowering all types of distortion including the one due to the output g_m. The above IM3 behavior

[4] This applies directly to g_m nonlinearity. From the data in Table III it can be observed that, with a gain of about 10, the second stage g_{ds} nonlinearity is of the same order of magnitude of its g_m nonlinearity. Hence, g_{ds} nonlinearity is also always negligible.

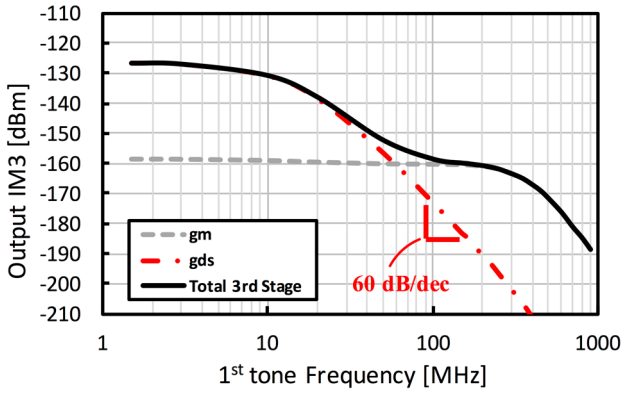

Fig. 9. Non-linear contributors of the output stage.

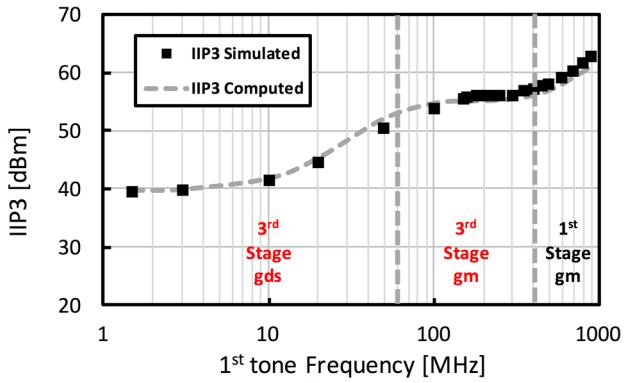

Fig. 10. Simulated IIP3 of the TIA, with the proposed OTA and dominating contributors

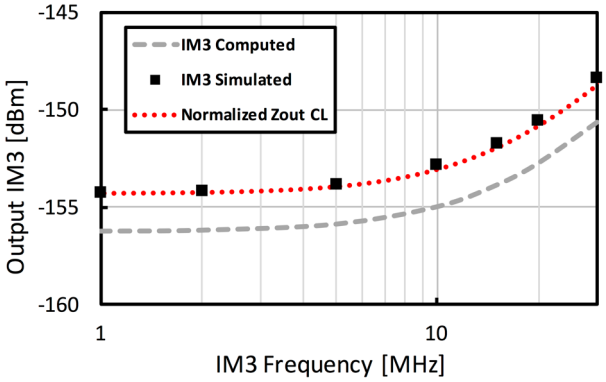

Fig. 11. IM3 as function of IM3 frequency and Closed-Loop output impedance frequency shape.

corresponds to the IIP3 shown in Fig. 10, where the dominant source of distortion in each frequency range is indicated. Lowering the TIA trans-impedance gain would lower IM3 injection and improve IIP3 up to 60 MHz, i.e. where the 3rd stage g_{ds} nonlinearity dominates. Beyond this frequency, a larger output stage or higher gain in front of it are needed to further boost IIP3. Our method allows also to compute IM3 vs. f_{IM3} to find the worst-case in-band distortion energy due to blockers at different relative frequencies. To do this, we place

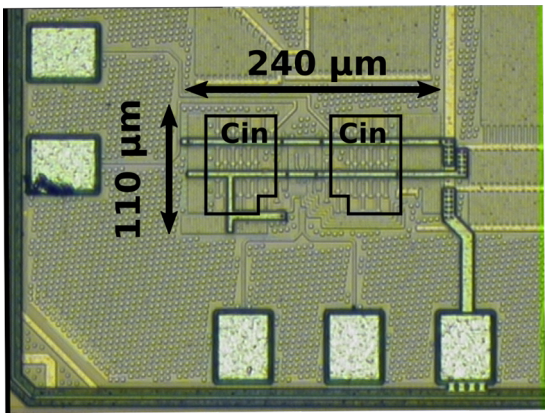

Fig. 12. Chip Photograph

the first tone at 100 MHz and move the second so that f_{IM3} is swept within the TIA band. In Fig. 11 we see that, as opposed to what generally happens, IM3 remains flat over almost all the TIA pass-band. This can be explained as follows. 1) In the frequency range considered output stage non-linearity is the main contributor. 2) The two tones are sufficiently beyond ω_0 that the g_m non-linearity dominates. 3) The non-linearity injection at f_{IM3} is independent of the position of the tones and the non-linear current is directly injected into the output node. 4) The IM3 follows the frequency shape of the closed loop output impedance, which is almost flat in-band since the first OTA pole is near 20 MHz.

Combining the results derived for both output and input stage we come to the following overall conclusions. To improve IIP3 we need to increase the OTA gain at the highest OOB blocker frequency for low input stage distortion and at ω_0 for low output stage distortion. This involves in general maximizing the OTA bandwidth but also shaping its frequency response to have a larger than 20 dB/decade slope up to as near as possible the OTA unity gain frequency while preserving TIA stability. The latter technique is especially necessary to cope with the input stage distortion. We notice that the presence of a wideband second stage is critical to achieve low IM3. In fact, it helps compressing the distortion from the output stage by increasing the in-band loop gain and it strongly reduces distortion injection from the first stage by reducing the OTA input signal.

V. Experimental Measurements

The photograph of the prototype TIA implemented in CMOS 28 nm is shown in Fig. 12. Thanks to the reduced input capacitance, area is only 0.026 mm^2. The measurement setup is shown in Fig. 13. An external balun converts the signal to differential while two 500 Ω resistors ($R_{d,SE}$) perform V-I conversion emulating the driving resistance of the passive mixer estimated from the LTE receiver in which the TIA is embedded. The output signal is detected with a differential active probe with a 2 pF differential load. The TIA frequency response, given in Fig. 14, has 20 MHz cut-off frequency and 14 dB in-band gain to represent an LTE channel. The output noise PSD, measured with 20 dB probe gain to overcome the

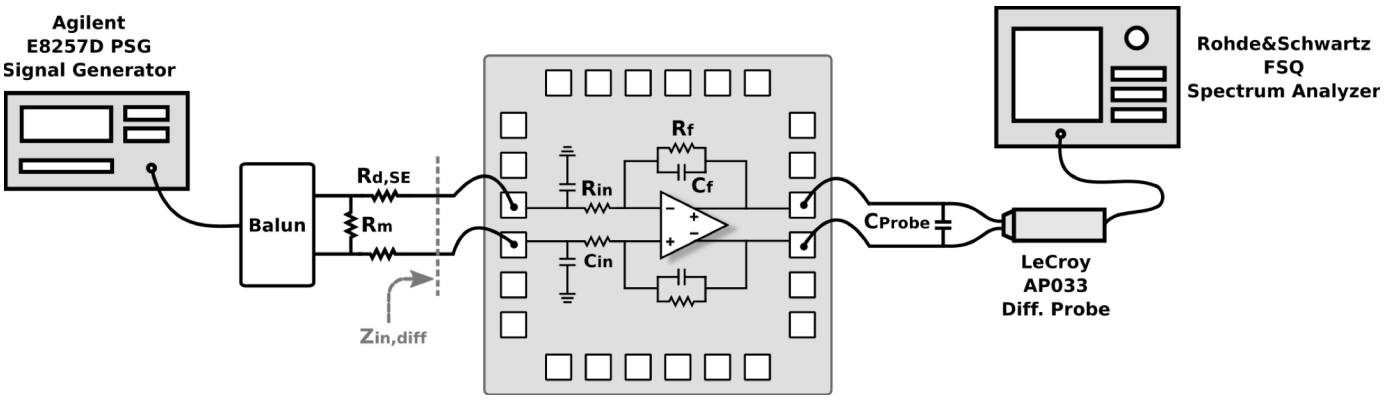

Fig. 13. Measurement Setup

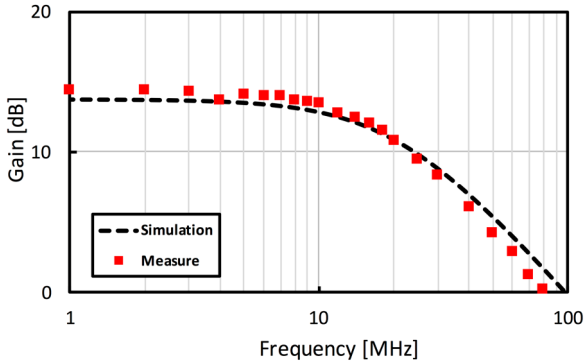

Fig. 14. Measured TIA Gain

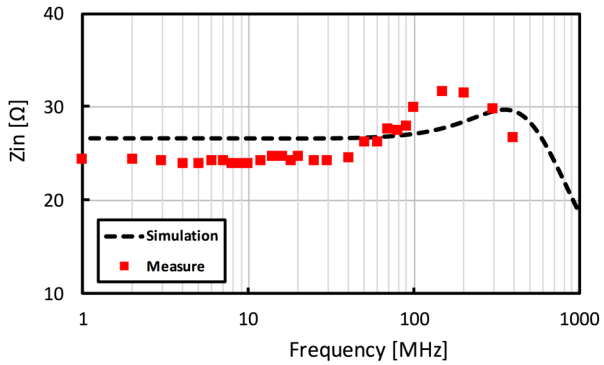

Fig. 16. Measured TIA Differential Input Impedance ($Z_{in,diff}$)

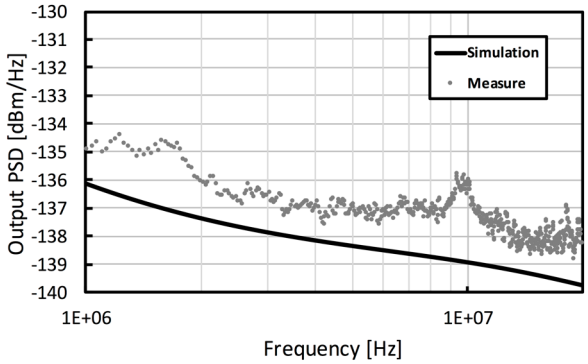

Fig. 15. Measured TIA Output Noise PSD

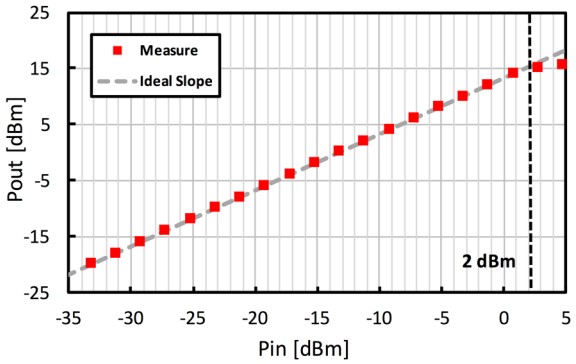

Fig. 17. Measured TIA 1-dB Compression

spectrum analyzer noise, given in Fig. 15 shows no in-band noise increase due to C_{in}. Main noise contributors are driving resistors, OTA and feedback resistors. The input-referred (IR) noise $P_{N,In}$ integrated up to 16 MHz is 21.1 μV_{RMS}. The differential TIA input impedance ($Z_{in,diff}$) was derived from s_{11} measurements with the 500 Ω driving resistances substituted with 50 Ω ones. From Fig. 16, the low frequency value is 25 Ω, almost entirely due to R_{in}, while the resistance at the virtual ground is only a few Ω. At higher frequency, due to OTA gain reduction, $Z_{in,diff}$ increases but stays always below 32 Ω, thanks to the large OTA bandwidth. For very high frequency C_{in} shunts the input, lowering $Z_{in,diff}$ again. Fig. 17 shows a 1-dB compression point of almost 2 dBm at 5MHz, corresponding to an output swing very close to the supply. Linearity was tested through a two-tone intermodulation test. A passive first order 3 MHz low-pass filter is used after the TIA, to limit the intermodulation of the probe for high frequency tones, where low IM3 signals have to be detected. Fig. 18 and 19 show the IIP3 for IB (5 MHz - 9 MHz) and OOB (100 MHz – 199 MHz) tones, respectively. Fig. 20 is a plot of measured and simulated IIP3 versus the first tone frequency, with IM3 always at 1 MHz. IIP3 starts from 31.5 dBm in-band, it increases moving out-of-band and reaches 50.5 dBm at 100 MHz[5]. IB IIP3 is around 9

[5] In [23] IR-noise and IIP3 were referred to the primary of the balun, performing a 1:3 impedance transformation.

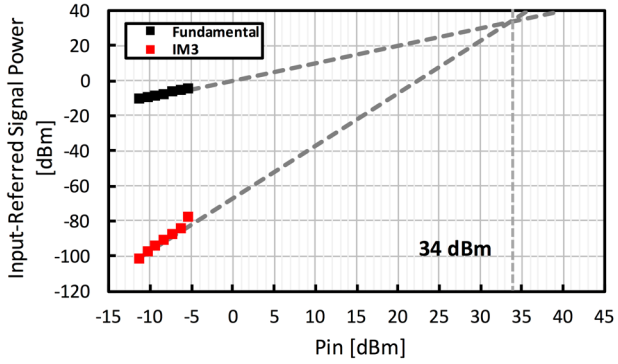

Fig. 18. IIP3 with Input signals at 5 MHz – 9 MHz

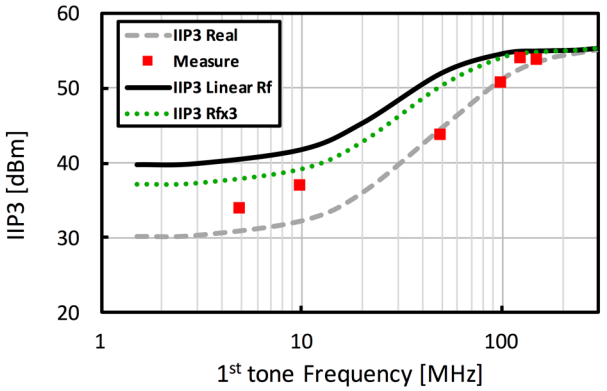

Fig. 20. IIP3 vs 1st tone frequency

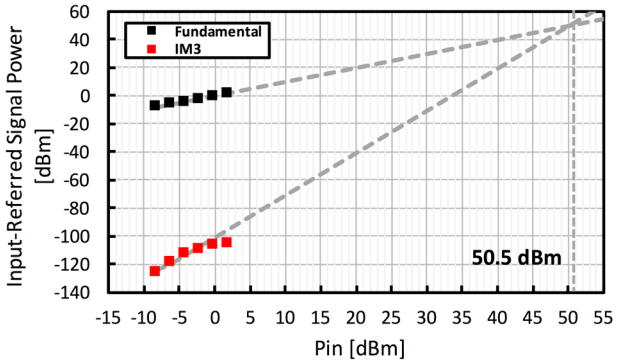

Fig. 19. IIP3 with input signals at 100MHz –199 MHz

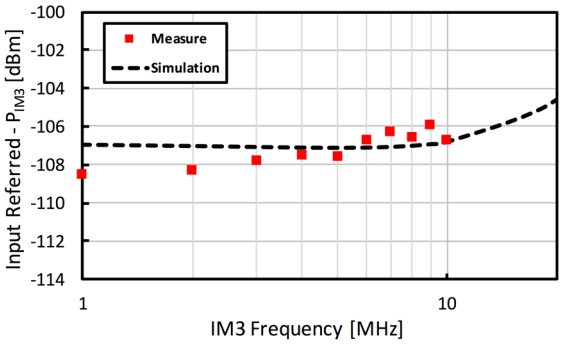

Fig. 21. IM3 vs IM3 frequency

TABLE V
TIA PERFORMANCE SUMMARY

Parameters	**This Work**	[12] RFIC '13	[13] ISSCC '16	[13] ISSCC '16	[14] JSSC '09	[15] JSSC '15	[32] JSSC '09	[32] JSSC '09
Technology [nm]	***28***	65	130	130	130	180	90	90
Area [mm^2]	***0.026***	0.29	0.45	0.45	1.53	0.14	0.5	0.5
Supply Voltage [V]	***1.8***	1.2	1.2	1.2	1	1.8	2.5	1.8
Power [mW]	***5.4***	3.4	1.92	1.92	7.5	1.38	1.26	0.15
f_0 [MHz]	***20***	14	2.8	12	5	33	2.8	2.8
N	***1***	5	2	2	5	4	4	4
OOB IIP3 [dBm]	***50.5***	20.6	48.5	36.1	52.8	18	35.6	48.5
Noise Vin [μV_{RMS}]	***21.1***	122	18.4	33.1	170	45	32	273
OOB IFDR [dB]	***87.5***	57.2	86.8	75.1	76.8	61.3	75	71.2
FOM_{conv} [$dB(J^{-1})$]	***183.2***	160.4	181.5	176.1	172	171.1	174.5	179.9
FOM_{IM3} [$dB(J^{-1})$]	***180.2***	155.9	174	172.3	165	155.9	167	172.4

$FoM_{conv} = IMFDR3|_{dB} + 10\log(N \cdot f_0/P_w)$ $FoM_{IM3} = FoM_{conv} + 10\log(f_{IM3}/f_0)$

dB smaller than expected (solid curve) when ideal feedback resistors are used in the TIA. Including the effect of poly-silicon feedback resistors non-linearity into the model (dashed curve) gives good correspondence. Multiplying by 3 the width of the poly resistors (dotted curve) less than 3 dB of in band degradation is incurred, showing that this is not a fundamental limit. The OOB IIP3 corresponds to an intermodulation-free dynamic range defined as $IMFDR_3|_{dB} = \frac{2}{3}(IIP3 - P_{N,In})$ of 87.5 dB [15]. OOB IIP3 was also tested vs. IM3 frequency, by moving the second-tone while keeping the first one at 100 MHz (Fig. 21). IM3 remains flat over almost all the filter band. This is consistent with the analysis of Section IV. TIA performance

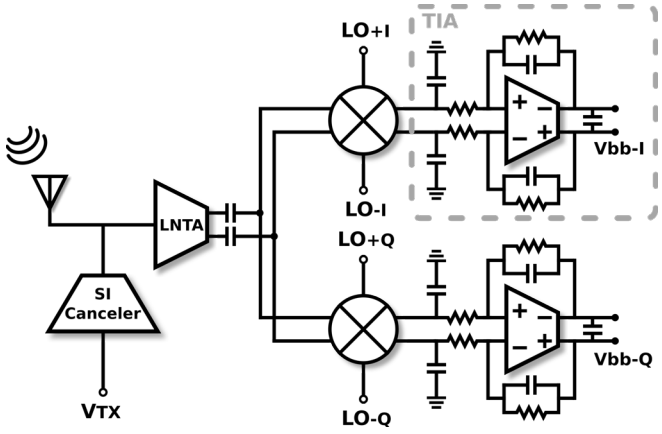

Fig. 22. Schematic diagram of the SI-Cancellation RX reported in [33]

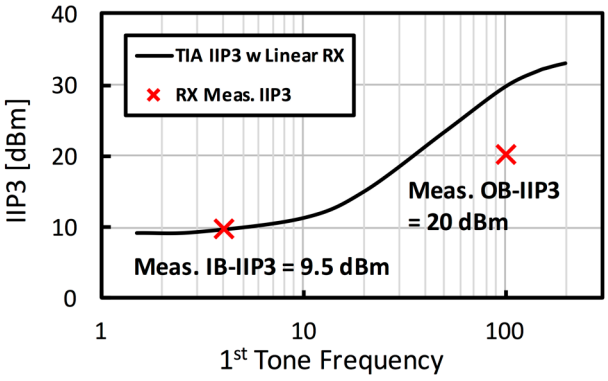

Fig. 23. RX IIP3 with perfectly linear LNTA and mixer (solid line) and measure IB and OOB RX IIP3.

is summarized and compared with other state-of-the-art filter implementations in Table V. Both Figure of Merit (FoM) given in [15] and reported in Table V are used for comparison. The proposed TIA has conventional and modified FOM's 2 dB and 6 dB above the previous best one [13], which has 7 times lower bandwidth. FOMs provide a useful way to compare different solutions given that high dynamic range is the key goal in a filter. This, however, assumes that noise and distortion can be freely traded with each other by changing the gain in front of the filter. On the other hand, in practical cases, there may be a maximum gain that can be achieved before other limitations occur. The TIA described in this paper is part of a highly-linear wideband receiver for FD and FDD wireless diversity [33] that includes a passive interference cancellation circuit and is conceptually shown in Fig. 22. The receiver LNTA is made of two complementary (p-n) cross-coupled common-gate (CG) amplifiers working in class-AB. The quadrature down-converter uses a passive mixer driven by a 25% duty-cycle LO, followed by the TIA, having a real pole at 20MHz. The TIA ensures a low loading impedance (< 32 Ohm) at the mixer output, while 20 pF capacitors to ground give a low impedance at very high frequencies (above 400 MHz). The chip, fabricated in 28nm CMOS, has a 0.51 mm^2 active area. The receiver s_{11} is below -10 dB from 1.5 to 3 GHz. At 2 GHz the gain and double-sideband (DSB) NF are 4.6 dB and 35 dB respectively. The receiver 1-dB compression point and IIP3 (without self-interference cancellation) are -15 dBm and 9.5 dBm respectively in-band while OOB (at 100 MHz offset) increase to 0 dBm and 19 dBm respectively. To assess the performance of the TIA in its real operating environment, we refer its noise and IIP3 to the receiver input. The TIA noise, referred to the receiver input corresponds to a DSB NF of 1.9 dB. It follows that the TIA contribution to the receiver NF is small. On the other hand, Fig. 23 (solid line) shows the impact of the TIA on the receiver IIP3, for the case of a perfectly linear LNTA and mixer. IIP3 starts from around 10 dBm IB and reaches 29 dBm at 100 MHz-offset. The much lower value of the TIA IIP3 when referred to the RX input is due to the > 20 dB difference between the gain from RX input to TIA output and the TIA gain. Fig. 23 clearly shows that the TIA is dominating IB receiver IIP3.

VI. Conclusions

A TIA for wireless receivers has been designed and tested. Avoiding any Miller capacitance but relying on zeros in both the OTA and the feedback, an outstanding bandwidth of 1.6 GHz was achieved. This allowed to reduce the capacitance at the TIA input from hundreds of pF to 20. The result is a better noise, a lower input impedance and a smaller distortion up to 400 MHz giving a FOM that exceeds that of all previous designs. Linearity optimization was made possible by a simple model capable to predict the IM3 of each stage and of each distortion mechanism within a stage.

Appendix A

This appendix describes how to extract the non-linear coefficients of each OTA stage. Equation (9) is derived from equation (3) with the gain G(ω) of each stage rewritten as $g_{m,i} \cdot |Z_{o,i}(\omega)|$. From (9) we see that when a stage is loaded by a low impedance, its g_m non-linearity is dominant since this reduces the output swing. On the contrary, when the load impedance is high, the large output swing makes the g_{ds} non-linearity dominant. With a 1 Ω load resistance at the stage output, (9) can be approximated by (10). Simulating the circuit intermodulation magnitude ($|v_{IM,out,i}|$) with two input tones of amplitude $A_{1,i}$ and $A_{2,i}$, the $g_{m,NL3,i}$ coefficient can be extracted by inversion of (10), as shown in (11).

$$v_{IM,out,i} = \left(\frac{3}{4} g_{m,3,i} {A_{1,i}}^2 A_{2,i} + \frac{3}{4} g_{ds,3,i} \left(A_{1,i} \cdot g_{m,i} \left|Z_{o,i}(\omega_1)\right|\right)^2 \cdot \left(A_{2,i} \cdot g_{m,i} \left|Z_{o,i}(\omega_2)\right|\right)\right) \cdot \left|Z_{o,i}(2\omega_1 - \omega_2)\right| \cdot \sin\left((2\omega_1 - \omega_2)t\right) \quad (9)$$

$$v_{IM,out,i} \cong \frac{3}{4} g_{m,3,i} {A_{1,i}}^2 A_{2,i} \cdot (1\Omega) \cdot \sin\left((2\omega_1 - \omega_2)t\right) \quad (10)$$

$$g_{m,3,i} \cong \frac{4}{3} \frac{|v_{IM,out,i}|}{{A_{1,i}}^2 A_{2,i} \cdot (1\Omega)} \quad (11)$$

The same simulation is performed with no explicit load. At sufficiently low frequency $Z_{o,i}(\omega)$ is the parallel of the r_{out} of the output transistors, which typically is in the order of kΩ. Putting

the result of (11) in (9) we get $g_{ds,3,i} = \frac{\frac{4\left|v_{IM,out,i}\right|}{3r_{o,i}} - g_{m,NL3,i}{A_{i,1}}^2 A_{2,i}}{{A_{1,i}}^2 A_{2,i}\left(g_{m,i}r_{o,i}\right)^3}$

.

REFERENCES

[1] M. Ramella, I. Fabiano, D. Manstretta and R. Castello, "A 1.7-2.1GHz +23dBm TX power compatible blocker tolerant FDD receiver with integrated duplexer in 28nm CMOS," *2015 IEEE Asian Solid-State Circuits Conference (A-SSCC)*, Xiamen, 2015, pp. 1-4.

[2] T. Zhang, A. R. Suvarna, V. Bhagavatula and J. C. Rudell, "An Integrated CMOS Passive Self-Interference Mitigation Technique for FDD Radios," in *IEEE Journal of Solid-State Circuits*, vol. 50, no. 5, pp. 1176-1188, May 2015.

[3] J. Zhou, T. H. Chuang, T. Dinc and H. Krishnaswamy, "Integrated Wideband Self-Interference Cancellation in the RF Domain for FDD and Full-Duplex Wireless," in *IEEE Journal of Solid-State Circuits*, vol. 50, no. 12, pp. 3015-3031, Dec. 2015.

[4] D. J. van den Broek, E. A. M. Klumperink and B. Nauta, "19.2 A self-interference-cancelling receiver for in-band full-duplex wireless with low distortion under cancellation of strong TX leakage," *2015 IEEE International Solid-State Circuits Conference - (ISSCC) Digest of Technical Papers*, San Francisco, CA, 2015, pp. 1-3.

[5] H. Zhang and E. Sanchez-Sinencio, "Linearization Techniques for CMOS Low Noise Amplifiers: A Tutorial," in *IEEE Transactions on Circuits and Systems I: Regular Papers*, vol. 58, no. 1, pp. 22-36, Jan. 2011.

[6] M. Valla, G. Montagna, R. Castello, R. Tonietto and I. Bietti, "A 72-mW CMOS 802.11a direct conversion front-end with 3.5-dB NF and 200-kHz 1/f noise corner," in *IEEE Journal of Solid-State Circuits*, vol. 40, no. 4, pp. 970-977, April 2005.

[7] H. Darabi, "Highly integrated and tunable RF front-ends for reconfigurable multi-band transceivers," *IEEE Custom Integrated Circuits Conference 2010*, San Jose, CA, 2010, pp. 1-8.

[8] I. Fabiano, M. Sosio, A. Liscidini, and R. Castello,"SAW-Less Analog Front-End Receivers for FDD and TDD," *IEEE Journal of Solid-State Circuits*, vol. 48, no. 12, Dec. 2013.

[9] Y. Lien, E. Klumperink, B. Tenbroek, J. Strange and B. Nauta, "A Mixer-First Receiver with Enhanced Selectivity by Capacitive Positive Feedback Achieving +39dBm IIP3 and <3dB Noise Figure for SAW-Less LTE Radio," in *Proc. IEEE Radio Frequency Integrated Circuits Symposium (RFIC)*, *RFIC '17*, Jun. 2017.

[10] D. Murphy, H. Darabi, A. Abidi, A. A. Hafez, A. Mirzaei, M. Mikhemar and M. –C. F. Chang, "A Blocker-Tolerant, Noise-Cancelling Receiver Suitable for Wideband Wireless Applications," *IEEE Journal of Solid-State Circuits*, vol. 47, no. 12, Dec. 2012.

[11] M. –D. Tsai, C. –F. Liao, C. –Y. Wang, Y. –B. Lee, B. Tzeng, and G. –K. Dehng, "A Multi-Band Inductor-Less SAW-Less 2G/3G-TD-SCDMA Cellular Receiver in 40nm CMOS," in *Proc. IEEE International Solid-State Circuits Conference (ISSCC), Feb. 2014, pp. 354-355.*

[12] M. Abdulaziz, A. Nejdel, M. Tormanen and H. Sjoland, "A 3.4mW 65nm CMOS 5th Order Programmable Active-RC Channel Select Filter for LTE Receivers," in *Proc. IEEE Radio Frequency Integrated Circuits Symposium (RFIC)*, *RFIC '13*, Jun. 2013, pp. 217-220.

[13] T. -Y. Liu, A. Liscidini, "A 1.92mW filtering transimpedance amplifier for RF current passive mixers", in *Proc. IEEE International Solid-State Circuits Conference (ISSCC), Feb. 2016, pp. 358-359.*

[14] H. Amir-Aslanzadeh, E. –J. Pankratz and E. Sanchez-Sinencio, "A 1-V +31 dBm IIP3, Reconfigurable, Continuously Tunable, Power-Adjustable Active-RC LPF," *IEEE Journal of Solid-State Circuits*, vol. 44, no. 2, Feb. 2009.

[15] M. De Matteis, A. Pezzotta, S. D'Amico and A. Baschirotto, "A 33 MHz 70 dB-SNR Super-Source-Follower-Based Low-Pass Analog Filter," *IEEE Journal of Solid-State Circuits*, vol. 50, no. 7, Jul. 2015.

[16] M. De Matteis; A. Pipino; F. Resta; A. Pezzotta; S. D'Amico; A. Baschirotto, "A 63-dB DR 22.5-MHz 21.5-dBm IIP3 Fourth-Order FLFB Analog Filter," in *IEEE Journal of Solid-State Circuits*.

[17] M. De Matteis, F. Resta, A. Pipino, S. D'Amico and A. Baschirotto, "A 28.8-MHz 23-dBm-IIP3 3.2-mW Sallen-Key Fourth-Order Filter With Out-of-Band Zeros Cancellation," in *IEEE Transactions on Circuits and Systems II: Express Briefs*, vol. 63, no. 12, pp. 1116-1120, Dec. 2016.

[18] S. D'Amico, M. Conta and A. Baschirotto, "A 4.1-mW 10-MHz Fourth-Order Source-Follower-Based Continuous-Time Filter With 79-dB DR," in *IEEE Journal of Solid-State Circuits*, vol. 41, no. 12, pp. 2713-2719, Dec. 2006.

[19] M. S. Savadi Oskooei, N. Masoumi, M. Kamarei and H. Sjoland, "A CMOS 4.35-mW +22-dBm IIP3 Continuously Tunable Channel Select Filter for WLAN/WiMAX Receivers," in *IEEE Journal of Solid-State Circuits*, vol. 46, no. 6, pp. 1382-1391, June 2011.

[20] J. Deguchi *et al*., "A Fully Integrated 2x1 Dual-Band Direct-Conversion Mobile WiMAX Transceiver With Dual-Mode Fractional Divider and Noise-Shaping Transimpedance Amplifier in 65 nm CMOS," in *IEEE Journal of Solid-State Circuits*, vol. 45, no. 12, pp. 2774-2784, Dec. 2010.

[21] D. H. Mahrof, E. A. M. Klumperink, Z. Ru, M. S. Oude Alink and B. Nauta, "Cancellation of OpAmp Virtual Ground Imperfections by a Negative Conductance Applied to Improve RF Receiver Linearity," in *IEEE Journal of Solid-State Circuits*, vol. 49, no. 5, pp. 1112-1124, May 2014.

[22] M. Abdulaziz, M. Tormanen and H. Sjoland, "A Compensation Technique for Two-Stage Differential OTAs," *IEEE Trans. Circuits Syst. II, Exp. Briefs*, vol. 60, no. 8, pp. 594–598, Aug. 2014.

[23] G. Pini, D. Manstretta and R. Castello, "Highly linear TIA for SAW-less FDD receivers," *2016 IEEE Asian Solid-State Circuits Conference (A-SSCC)*, Toyama, 2016, pp. 117-120.

[24] H. Khatri, P. S. Gudem and L. E. Larson, "Distortion in Current Commutating Passive CMOS Downconversion Mixers," in IEEE Transactions on Microwave Theory and Techniques, vol. 57, no. 11, pp. 2671-2681, Nov. 2009.

[25] M. Sosio, A. Liscidini, and R. Castello, *"An Intuitive Current-Driven Passive Mixer Model Based on Switched-Capacitor Theory," IEEE Trans. Circuits Syst. II, Exp. Briefs*, vol. 60, no. 2, pp. 66–70, Feb. 2013.

[26] E. Sacchi, I. Bietti, S. Erba, L. Tee, P. Vilmercati and R. Castello, "*A 15 mW, 70 kHz 1/f Corner Direct Conversion CMOS Receiver*," in Proc. IEEE Custom Integrated Circuits Conference (CICC), Sep. 2003, pp. 459-462.

[27] P. Wambacq, W. Sansen, *Distortion Analysis of Analog Integrated Circuits*, 1st ed., Norwell, MA: Kluwer Academic Publishers, 1998.

[28] P. Wambacq, G. G. E. Gielen, P. R. Kinget and W. Sansen, "High-Frequency Distortion Analysis of Analog Integrated Circuits," *IEEE Trans. Circuits Syst. II, Exp. Briefs*, vol. 46, no. 3, pp. 335–345, Mar. 1999.

[29] B. Hernes and W. Sansen, "Distortion in Single-, Two- and Three-Stage Amplifiers, " in *IEEE Transactions on Circuits and Systems I: Fundamental Theory and Applications*, vol. 52, no. 5, pp. 846-856, May 2005.

[30] G. Palumbo and S. Pennisi, "High-frequency harmonic distortion in feedback amplifiers: analysis and applications," in *IEEE Transactions on Circuits and Systems I: Fundamental Theory and Applications*, vol. 50, no. 3, pp. 328-340, Mar 2003.

[31] N. Krishnapura and K. S. Rakshitdatta, "A Model-Agnostic Technique for Simulating Per-Element Distortion Contributions," in IEEE Transactions on Circuits and Systems I: Regular Papers, vol. 61, no. 8, pp. 2219-2228, Aug. 2014.

[32] A. Pirola, A. Liscidini and R. Castello, "Current-Mode, WCDMA Channel Filter With In-Band Noise Shaping," *IEEE Journal of Solid-State Circuits*, vol. 45, no. 9, Sep. 2010.

[33] E. Kargaran, S. Tijani, G. Pini, D. Manstretta and R. Castello, "Low Power Wideband Receiver with RF Self-Interference Cancellation for Full-Duplex and FDD Wireless Diversity," in *Proc. IEEE Radio Frequency Integrated Circuits Symposium (RFIC)*, *RFIC '17*, Jun. 2017.

Giacomo Pini (S'16) was born in Pavia, Italy, in 1990. He received the M.Sc. degree (*cum laude*) in Miroelectronic Engineering at the University of Pavia, Italy, in 2015, where he is currently working towards the Ph.D. degree.

His research interests include base-band filters for broadband wireless receivers.

Danilo Manstretta (M'03) received the Laurea (summa cum laude) degree and the
Ph.D. degree in electrical engineering and computer science from the University of Pavia, Pavia, Italy, in 1998 and 2002, respectively.

He was involved in CMOS RF front-end circuits for direct-conversion wireless applications. From 2001 to 2003, he was a Member of Technical Staff with Agere Systems, Murray Hill, NJ, USA. where he was involved in WLAN transceivers and linear power amplifiers for base stations. From 2003 to 2005, he was with Broadcom Corporation, Irvine, CA, USA, where he was involved in RF tuners for TV applications. In 2005, he joined the University of Pavia as an Assistant Professor, and was granted tenure in 2008. His current research interests include the field of analog, RF, and millimeter-wave integrated circuit design.

Dr. Manstretta was a co-recipient of the 2003 IEEE JOURNAL OF SOLID-STATE CIRCUITS BEST PAPER AWARD. He has been a Member of the Technical Program Committee of the IEEE Radio Frequency Integrated Circuits Symposium since 2006 and of the Steering Committee for the same conference since 2017. He was a Guest Editor of the IEEE JOURNAL OF SOLID-STATE CIRCUITS May 2017 Special Section dedicated to the 2016 RFIC Symposium.

Rinaldo Castello (S'78–M'78–SM'92–F'99) received the bachelor's (summa cum laude) degree from the University of Genova, Genoa, Italy, in 1977, and the M.S. and Ph.D. degrees from the University of California, Berkeley, CA, USA, in 1981 and 1984, respectively.

From 1983 to 1985, he was a Visiting Assistant Professor with the University of California. In 1987, he joined the University of Pavia, Pavia, Italy, where he is currently a Full Professor. He consulted for ST-Microelectronics, Milan, Italy until 2005. In 1998, he started the Joint Research Centre between the University of Pavia and ST-Microelectronics and was its Scientific Director until 2005. He promoted the establishing of several design center from multinational IC companies around Pavia, among them Marvell for which he was a consultant from 2005 to 2016. He is currently consulting for InvenSense, Milano, Italy.

Prof. Castello was named one of the Outstanding Contributors for the first 50 and 60 years of ISSCC. He was a co-recipient of the Best Paper Award at the 2005 Symposium on VLSI of the Best Invited Paper Award at the 2011 CICC and of the Best Evening Panel Award at ISSCC 2012 and 2015. He has been a TPC Member of the European Solid State Circuit Conference (ESSCIRC) since 1987 and of the International Solid State Circuit Conference (ISSCC) from 1992 to 2004. He was the Technical Chairman of ESSCIRC in 1991, the General Chairman of ESSCIRC 2002, an Associate Editor for Europe of the IEEE JOURNAL OF SOLID-STATE CIRCUITS from 1994 to 1996, and Guest Editor of its in 1992 special issue. From 2000 to 2007, he was a Distinguished Lecturer of the IEEE Solid State Circuit Society. He was one of the two European representatives at the Plenary Distinguished Panel of ISSCC 2013 and the 2014 Issue of the IEEE SOLID STATE CIRCUIT MAGAZINE was devoted to him.